CORROSION SCIENCE AND TECHNOLOGY, Vol.24, No.3(2025), pp.134~150 pISSN 1598-6462 / eISSN 2288-6524
[Research Paper] DOI: https://doi.org/10.14773/cst.2025.24.3.134

Evaluating the Potential of Ataluren as X80 Steel Corrosion Inhibitor in Acid Wash Solution: An Experimental and Computational Intelligence Approach

Ekemini Ituen[1,2,†], Victor Mkpenie[1,2], Solomon Shaibu[1,2], Lin Yuanhua[3,†], Udoinyang Inyang[4], Shuangqin Sun[5], Simphiwe Nelana[6], Michael Klink[6], and Olushola Ayanda[7,†]

[1]*Computational Materials Science Group, TETFund Center of Excellence in Computational Intelligence, University of Uyo, Uyo, Nigeria*
[2]*Materials and Oilfield Chemistry Group, Department of Chemistry, Faculty of Physical Science, University of Uyo, Uyo, Nigeria*
[3]*State Key Laboratory of Oil and Gas Reservoir Geology and Exploitation, Southwest Petroleum University, Chengdu 610500, Sichuan, China*
[4]*Department of Data Science, Faculty of Computing, University of Uyo, Uyo, Nigeria*
[5]*School of Materials Science and Engineering, China University of Petroleum (East China), Qingdao, Shandong 266580, China*
[6]*Department of Chemistry, Vaal University of Technology, Vanderbijlpark, South Africa*
[7]*Department of Chemistry, Federal University Oye-Ekiti, Oye-Ekiti, Nigeria*
(Received October 28, 2024; Revised December 23, 2024; Accepted April 15, 2025)

Corrosion inhibition performance of Ataluren (ATA) on X80 steel in oilfield acid wash solution was investigated using a combination of experimental and computational techniques. Corrosion rates were quantified using weight loss analysis and electrochemical methods. Surface morphology and protection mechanisms were examined using spectroscopic and microscopic tools. Quantum chemical calculations and molecular dynamics simulations were performed to evaluate solvation, adsorption behavior, and binding affinity of ATA molecules at the steel interface. Experimental results demonstrated significant reductions of corrosion rates across various ATA concentrations, achieving inhibition efficiencies of 96.2%, 95.6%, and 96.3% as determined by impedance, polarization and weight loss measurements, respectively, while Monte Carlo simulations supported an inhibition efficiency of 76.1%. Analysis of Fukui indices, Mulliken charge distributions and interaction energies in both gas and aqueous phases, along with EDAX data, indicated that corrosion inhibition was primarily driven by spontaneous exothermic chemisorption involving N and O functionalities in ATA interacting with Fe d-orbitals. This adsorption led to formation of a protective ATA monolayer that significantly reduced surface roughness, as confirmed by SEM. These findings establish ATA as a highly effective corrosion inhibitor for X80 steel under investigated conditions.

Keywords: *Adsorption, Corrosion protection, DFT, Interaction energy, Surface characterization*

1. Introduction

Acidizing is a common procedure in the petroleum industry. The primary aim of acidizing is to enhance well output by eliminating drilling-related defects or by enhancing the physical attributes of the reservoir rock, such as its porosity and permeability. Acid wash and well stimulation are the various forms of acidizing requiring pumping of acid into a drilled well to clean the well of scales, debris, deposits or to etch the formation rocks, enlarge flow channels and improve hydrocarbons production. The nature and concentration of the acid deployed for the acidizing procedure is often determined by the formation geology and the type of acidizing to be carried out [1]. For acid wash or descaling procedure, mild hydrochloric acid (HCl) of about 5 % concentration is commonly used [2]. The 5 % HCl solution reacts with calcium scales, dissolves it to produce calcium chloride salt, carbon (IV) oxide and water according to equation (1).

$$HCl + CaCO_3 \rightarrow CaCl_2 + CO_2 + H_2O \quad (1)$$

The use of HCl is desirable because it reacts very fast and completely with the calcium rocks before becoming spent. However, being very corrosive, it causes corrosive damage to surfaces of steel pipes and casing, and with time, could lead to materials failure. Materials failure

†Corresponding author: ekeminiituen@uniuyo.edu.ng, lin28@126.com, osayanda@gmail.com

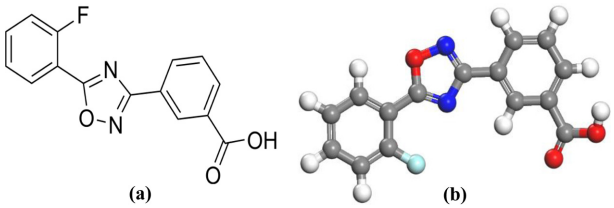

Fig. 1. (a) Molecular structure of ATA and (b) Structure of ATA optimized at DFT/6-311G(d,p). (O: red; N: blue; C: grey; H: white; F: light green)

may be disastrous and has to be prevented, hence corrosion inhibitors are often added to the acid to slow down corrosion and protect materials integrity [3]. Although several corrosion inhibitors (CIs), their behaviours and inhibition efficiencies in various acidizing conditions have been reported in literature [4-7], the search for alternative CIs that are cost effective, highly efficient, sustainable and environmentally friendly is still very active.

Corrosion inhibition of X80 steel have been mitigated by employing organic inhibitors (such as amine derivatives), surfactants, and plant extracts, as well as inorganic compounds like phosphates and molybdates. Polymer based inhibitors, nanomaterials and composite systems also offer protection of X80 steel [8-10]. These materials form protective layers on the steel surface, reducing corrosion rates, especially in pipeline applications exposed to harsh conditions. In the present study, we present the results of our investigation of ataluren (ATA) as an alternative CI for X80 steel in simulated acid wash solution. The aim of this study was to assess the effectiveness of ATA in inhibiting steel corrosion in oilfield environment, so that subsequently, ATA could be used as the active ingredient for formulating anticorrosion oilfield chemical.

ATA is a pharmaceutical drug used for the treatment of some renal and muscular issues and is not known for any toxic effects [11,12]. The choice of ATA was motivated by its molecular structure which contains aromatic and heterocyclic rings with nitrogen atoms, oxygen atoms and continuous conjugated double bonds system (Fig. 1). These sites are electron rich in nature, and have been adjudged as potential sites for attachment of CI molecules on surfaces they are deployed to protect through the adsorption mechanism [13].

2. Experimental

2.1 Preparation of test solutions

ATA (CAS No. 775304-57-9, Purity - 98%, Solubility - 30 mg/mL) and hydrochloric acid (37% HCl) were supplied by Double Bond Chemicals, Uyo, Nigeria and were used to prepare the test solutions as supplied. The acid was diluted to concentration of 5 % HCl to simulate oilfield acid wash solution [14]. Appropriate masses of ATA were used to prepare different concentrations (1.0 mM to 10.0 mM) of ATA in the simulated acid wash solution. Double deionized water was used for all the preparations. Models of equipment used are presented in supplementary file (**Sup-1**).

2.2 Steel specimens preparation

Casing and pipework steel were simulated using X80 steel coupons of composition (wt%) C (0.17), Mn (1.25), Si (0.38), Mo (0.20), P (0.015), Ti (0.015), S (0.002), Nb (0.04), Fe (balance) quoted and supplied by Shengxin Technology Co. Ltd, Xinyang, China. The coupons were cleaned by following the ASTM recommended routine for cleaning steel coupons to be used in corrosion experiments [15]. In addition, coupons were abraded to mirror finishing using different grades of silicon carbide paper (CC-22F P2000 grade). Coupons for electrochemical experiments were of sizes 1 cm × 1 cm × 0.25 cm, and were almost entirely insulated using epoxy resins mixture but 1 cm^2 surface area was exposed. Coupons used for weight loss experiment were 2 cm × 2 cm × 0.25 cm in dimension.

2.3 Electrochemical tests

Electrochemical impedance spectroscopy (EIS) was conducted at 303 K using Gamry workstation and the set up consists of saturated calomel electrode as reference, X80 steel coupon as working electrode and platinium electrode as counter electrode. Time for open circuit potential (OCP) was set at 1800 s and frequency range at 100 kHz - 10 mHz. Potentiodynamic polarization was conducted at voltage range of −0.15 V - + 0.15 V vs. OCP and scan rate = 0.2 mV/s [16]. Obtained data was tested in various equivalent circuit models with E-Chem software to elucidate electrochemical parameters of interest. Triplicate measurements were taken, all at

room temperature, and results obtained in each measurement were averaged and reported with errors. The average values of charge transfer resistance (R_{ct}) and corrosion current (I_{corr}) obtained from electrochemical impedance spectroscopy (EIS) (I_e) and PP (I_p) tests were inputted into equations (2) and (3) respectively to determine the percentage inhibition efficiency [17].

$$I_e = 100\left(\frac{R_{ct0} - R_{ct1}}{R_{ct1}}\right) \quad (2)$$

$$I_p = 100\left(1 - \frac{I^1_{corr}}{I^0_{corr}}\right) \quad (3)$$

Given that R_{ct0} and R_{ct1} stands for the charge transfer resistance without and with the additives respectively, and I^0_{corr} and I^1_{corr} stands for the corrosion current obtained without and with the additives respectively.

2.4 Weight loss test

The initial weight (w_o) of each X80 steel coupon was recorded, then the coupon was totally immersed in 50 mL of each test solution. The vessel was then sealed to simulate absence of air and maintained at 303K in a water bath for 5 h. Thereafter, the coupons were retrieved, cleaned according to ASTM G1-03 (2017)e1 procedures and the new weight (w_1) was recorded. The difference in weights (weight loss, in grams) ($\Delta w = w_o - w_1$) was recorded. This was repeated in triplicates for the different test solutions and at other temperatures (313, 323 and 333 K). The mean of the obtained weight losses were used to compute the corrosion rate (CR (cmh^{-1})) and inhibition efficiency (I_w) using equations (4) and (5), respectively

$$CR = \frac{87600\Delta w}{\rho A t} \quad (4)$$

$$I_w(\%) = 100\left(1 - \frac{CR_1}{CR_0}\right) \quad (5)$$

where CR_1 stands for corrosion rate when ATA were used and CR_0 stands for corrosion rate in 5% HCl without ATA, ρ stands for the density (g·cm^{-3}) of iron, A stand$_t$ for the cross sectional area (cm^2) of the coupon and stands for the immersion time (h). The obtained CR values were multiplied by 8.76×10^4 being a factor that converts the initial value to mmy$^{-1.}$ [18].

2.5 Surface morphology and corrosion products analyses

The morphologies of the X80 steel specimens retrieved from the inhibited and uninhibited solutions were determined by SEM following standard procedures described in literature [19]. Moreover, the elemental composition on the surface of the retrieved X80 steel coupons were checked by EDAX and compared.

2.6 Computational method

2.6.1 Quantum chemical calculation

Quantum chemical parameters of ATA were computed using its optimized structure. The geometry optimization achieved with B3LYP method [20] and 6-311G (d, p) basis set was implemented within the density functional theory (DFT) framework using Gaussian 09 program package [21]. Aqueous phase calculation was realized using the integral equation formalism variant of Polarizable Continuum Model (IEFPCM) [22]. The energies of the highest occupied molecular orbital (E_{HOMO}) and lowest unoccupied molecular orbital (E_{LUMO}) were obtained and used subsequently to calculate other quantum chemical parameters such as ionization energy (IE) electron affinity (EA), energy gap (E_{gap}), electronegativity (χ), global hardness (η) and global softness (σ), respectively as shown in equations (6) ~ (11).

$$\Delta E = E_{LUMO} - E_{HOMO} \quad (6)$$

$$IE = -E_{HOMO} \quad (7)$$

$$EA = -E_{LUMO} \quad (8)$$

$$\chi = \frac{1}{2}(IE + EA) \quad (9)$$

$$\eta = \frac{1}{2}(IE - EA) \quad (10)$$

$$\sigma = \frac{1}{\eta} \quad (11)$$

where HOMO and LUMO represents the highest occupied molecular orbital and the lowest unoccupied molecular orbital respectively, The number of electrons transported between ATA and Fe surface, ΔN was calculated using the equation (12).

$$\Delta N = (\varphi - \chi_i)/2\eta_i \quad (12)$$

Here, η_i and χ_i are global hardness and electronegativity of ATA, respectively while φ is the work function of Fe surface and is given a value of 4.82 [23].

2.6.2 Construction of simulation box

In the experimental corrosion studies, steel coupons are often consistently immersed in corroding solution containing the inhibitor, indicating the thorough saturation of the steel under examination. This practice contrasts with the usual computational simulations where the solution is often placed on the steel surface [24]. To submerge the steel, a Fe crystal was cleaved at the (110) crystal plane, resulting in a 1 Å thick layer of Fe atoms, akin to a single strip of a steel coupon. To accommodate ATA without periodic interaction, a supercell measuring 11 × 11 $Å^2$ was created from the cleaved Fe surface, providing ample space. A vacuum slab with a thickness of 30 Å was generated from the supercell, positioned centrally in the simulation box at 15 Å. The resulting simulation box was of dimensions 27.30 × 27.30 × 30.00 $Å^3$.

2.6.3 Composition of inhibitor solution and packing of molecules into the simulation box

The number of molecules of ATA, HCl and H_2O was determined and compared based on a 50 mL 5% HCl solution used for the experimental investigation. Interestingly, the HCl molecule count is slightly less than that of H_2O, suggesting approximately 90.41% protonation of the entire water molecule. Since hydrogen ions (H^+) do not exist independently in solution, the number of dissociated H^+ ions is equivalent to those added to H_2O, forming hydronium ions (H_3O^+). Notably, some H_2O molecules remain unprotonated in this process. This information provides insights into the protonation behavior in the HCl solution and the resulting hydronium ion formation.

Using the simulation box created earlier, the molecules of ATA, H_3O^+, Cl^- and H_2O were packed using the Amorphous Cell of Materials Studio with a density of 1.0 g/cm^3. A Connolly surface of radius, 1 Å, was created, and the molecules were efficiently arranged within the isosurface enclosed volume. This iso-surface accurately represents the volume where the Fe atoms are situated, ensuring that the Fe surface is fully immersed in the inhibitor solution. To achieve a precise composition, the quantities of ATA, H_3O^+, Cl^-, and H_2O were adjusted based on their mole ratio and available space. The inhibitor solution was meticulously packed into the Connolly surface, adhering to the specified composition: 1 ATA, 211 H_3O^+, 211 Cl^-, and 22 H_2O. This meticulous arrangement maintains a protonation level of 90.41% in the aqueous medium, ensuring the efficacy of the inhibitor solution and simulating experimental conditions as closely as possible.

2.6.4 Molecular dynamics (MD) simulation

The packing of inhibitor solution into the Fe cell resulted in the formation of Fe-ATA system. This system was optimized using Forcite engine employing Smart algorithm, COMPASS forcefield and convergence criteria of 1.0×10^{-4} kcal/mol (energy), 5.0×10^{-3} kcal/mol/Å (force) and 5.0×10^{-5} Å (displacement). Geometry optimization was achieved in 5895 iteration steps. The optimized Fe-ATA system was subjected to molecular dynamics (MD) simulation task employing NVT (constant number of molecules, constant volume and constant temperature) ensemble with a time step of 1.0 fs and total simulation time of 50.0 ps. The temperature for MD simulation was adjusted according to the experimental temperatures of 303 - 333K respectively while exchange of heat with the environment was controlled by Nose thermostat. The structure obtained from MD simulation stage was utilized for single point energy calculation. The energy of interaction was determined from equation (13):

$$E_{int} = E_{total} - (E_{Fe+solu} + E_{inh+solu} - E_{solu}) \quad (13)$$

Here, E_{int} is the energy of interaction between the Fe and ATA, E_{total} is the total energy of the Fe-ATA system, $E_{Fe+solu}$ is the energy of Fe and acid solution, $E_{inh+solu}$ is the energy of inhibitor and acid solution and E_{solu} is the energy of the acid solution.

The inhibition efficiency was also calculated theoretically using equation (14):

$$E_{inh}\% = (E_o - E_i) / E_o \quad (14)$$

Here, E_{inh}% is the inhibition efficiency of ATA on Fe(110) surface, E_i is the interaction energy computed

from equation (13) (with inhibitor) and E_o is the interaction energy obtained without inhibitor in the acid solution. E_o can be determined according to equation (15):

$$E_o = E_{Fe+solu} - (E_{Fe} + E_{solu}) \quad (15)$$

Here, $E_{Fe+solu}$ represents the total energy of Fe(110) surface in acid solution without any inhibitor, E_{Fe} is the energy of Fe(110) surface while E_{solu} is the energy of the acid solution.

3. Results and Discussion

3.1 Open circuit potential

The obtained open circuit potential (OCP) values were plotted against time as shown in Fig. 2a. As can be observed from that plot, for all the solutions tested, OCP attained reasonable stability after 600 s. With the solutions containing ATA, the OCP values were more negative compared to the blank 5% HCl solution. Such shift of voltage response to cathodic region on addition of the inhibitor, though not a sufficient criterion, provides a clue that ATA could be a cathodic corrosion inhibitor [25].

3.2 EIS study

The imaginary and real components of impedance obtained from EIS experiment were used to plot the Nyquist curves shown in Fig. 2c. The plot yields depressed semi-circular curves with a single relaxation time constant. This shape is similar to those obtained from EIS study of some other corrosion inhibitors reported in literature and is often associated with charge transfer controlled mechanism [26,27]. Since all the curves are similar in shape, it therefore implies that the corrosion process occurs through a similar mechanism despite the addition of ATA. However, the diameters of the semicircular curves vary in magnitude, the smallest

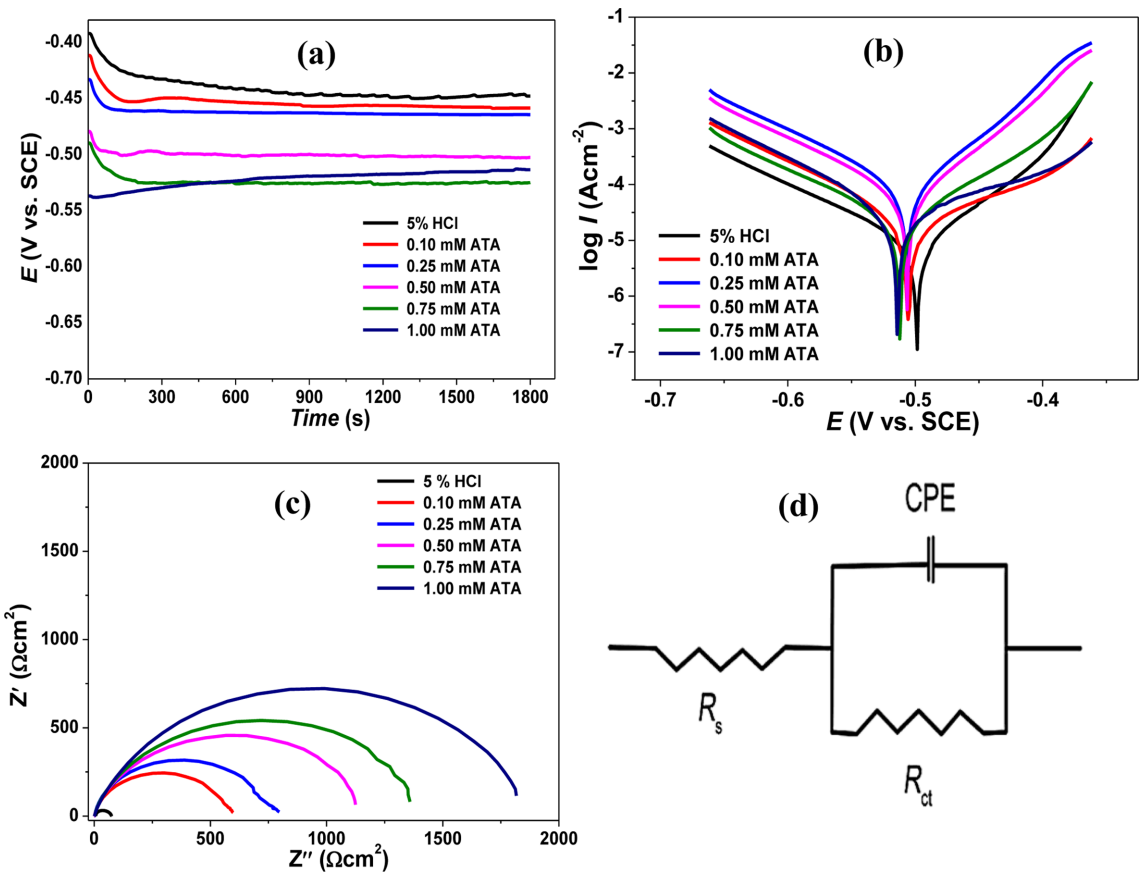

Fig. 2. (a) OCP vs. time plot (b) Tafel polarization curves (c) Nyquist curves and (d) Equivalent circuit model for the corrosion of X80 steel surface in 5% HCl without and with different concentrations of ATA

Table 1. Some parameters deduced form EIS measurement

Test solutions	R_s (Ωcm^2)	R_{ct} (Ωcm^2)	n	C_{dl} ($\mu F cm^{-2}$)	χ^2 (10^{-4})	I_{EIS} (%)
5 % HCl	3.1±0.3	74.2±2.2	0.81	26.07	2.66	-
0.10 mM ATA	2.0±0.2	597.8±2.6	0.85	18.91	4.13	87.6
0.25 mM ATA	1.8.±0.2	797.5±5.3	0.86	16.09	9.78	90.7
0.50 mM ATA	1.7±0.3	1125.4±3.1	0.88	11.46	4.65	93.4
0.75 mM ATA	1.6±0.2	1359.7±11.8	0.88	9.08	11.72	94.5
1.00 mM ATA	1.3±0.2	1945.2±4.3	0.89	5.22	3.84	96.2

obtained with 5% HCl while the highest was obtained with the solution containing 1.0 mM ATA. The diameter corresponds to charge transfer resistance and increases as concentration of ATA increases, which may be attributed to adsorption of ATA molecules to form a thin film on the surface of the steel electrode [28].

In order to quantitatively determine key parameters (Table 1) associated with the impedance measurement, the data obtained was fitted into various equivalent circuit models. The model shown in Fig. 2d consisting of the constant phase element (CPE), solution resistance (R_s) and charge transfer resistance (R_{ct}), afforded the best fit with χ^2 values between 1.2×10^{-3} to 0.4×10^{-3}. The magnitude of R_{ct} depicts the extent of opposition to current flow through the electrode surface by the adsorbed surface film of ATA molecules. Since it increases as the concentration of ATA increases, it implies that the protective property of the adsorbed ATA film improves as more ATA molecules are added per unit volume of the electrolyte. In other words, increase in concentration of ATA increases the surface coverage of ATA molecules on the steel surface, thereby increasing insulation property of the adsorbed film towards the aggressive electrolyte. As more ATA molecules are adsorbed, water molecules (initially adsorbed) are displaced therefore reducing the corrosion rate [28].

3.3 Potentiodynamic polarization study

The effect of ATA addition on the corrosion current and voltage responses was investigated by potentiodynamic polarization technique. The polarization curves shown in Fig. 2b were obtained from which some associated parameters displayed in Table 2 were deduced. It can be observed that the curves representing the solutions with ATA are displaced towards the left with respect to that of the 5% HCl solution and their respective E_{corr} values are more negative than that of 5% HCl. This is an indication that ATA exhibits more cathodic effect by mechanism. However, the extent of displacement of E_{corr} (5% HCl) from all the ATA solutions is within the range of ±85 mV which is assigned to mixed type inhibitor mechanism [29]. By considering the displacement towards cathodic region, ATA can be categorized as mixed type inhibitor but having cathodic predominance [30]. The cathodic predominance is further demonstrated in the values of β_c which does not follow a consistent trend compared to β_a. Also, the corrosion current measured with the inhibited solutions are smaller in magnitude than that of 5% HCl solution. This could have been due to local insulation of the steel surface by adsorbed surface adsorbed molecules and consequent resistance to current passage. From this behaviour, inference can be drawn that the adsorption of ATA molecules on the steel surface resulted in the reduction of corrosion current, hence inhibition of the corrosion process. As can be inferred from the corrosion current response against ATA concentration, increase in ATA concentration affords more ATA molecules (at the interface) available for adsorption resulting in higher inhibition efficiency. Thus, the inhibition efficiency of ATA increases as its concentration increases, similar to and supporting the trend obtained from EIS study [31].

3.4 Weight loss

Concentrated acid solutions are known to be corrosive and the corrosive attack causes gradual dissolution of the steel material immersed in the acid. Weight loss

Table 2. Some parameters deduced from potentiodynamic polarization measurement

Test solutions	E_{corr} (V)	I_{corr} (Acm^{-2})	β_a (mVdec^{-1})	β_c (mVdec^{-1})	I_{PDP} (%)
5 % HCl	-0.458	826.2±2.7	152.1	143.5	-
0.10 mM ATA	-0.505	142.3±1.9	156.4	157.1	83.5
0.25 mM ATA	-0.506	93.1±1.6	159.3	128.6	89.2
0.50 mM ATA	-0.512	72.4±1.8	166.9	128.4	91.6
0.75 mM ATA	-0.514	57.8±1.6	169.2	141.3	93.3
1.00 mM ATA	-0.518	37.9±1.7	180.4	148.7	95.6

Table 3. Mean values of corrosion rate and inhibition efficiency obtained for the different test solutions at different temperatures by weight loss measurement

Test solution	Corrosion rate (mmy^{-1})				Inhibition efficiency (%)			
	303 K	313 K	323 K	333 K	303 K	313 K	323 K	333 K
5 % HCl	8.82	11.91	17.63	26.19	-	-	-	-
0.10 mM ATA	1.25	2.05	3.47	5.66	85.8	82.8	80.3	78.4
0.25 mM ATA	1.11	1.76	3.07	5.05	87.4	85.2	82.6	80.7
0.50 mM ATA	0.74	1.26	2.57	4.82	91.6	89.4	85.4	81.6
0.75 mM ATA	0.52	0.87	2.01	4.09	94.1	92.7	88.6	84.4
1.00 mM ATA	0.33	0.53	1.53	2.99	96.3	95.1	91.3	88.6

technique affords a direct method for determining the amount of the steel dissolved by the corrosive acid at a given time and temperature. The average losses in weights of the coupons in the different test solutions were obtained and used to calculate the values of the corrosion rates shown in Table 3. The corrosion rate was highest in the 5% HCl and increased with temperature which is thermodynamically consistent. Addition of ATA resulted in a decrease in corrosion rate in an inverse concentration dependent manner. Even at concentration as low as 1.0 mm, ATA afforded 96.3% and 88.6% efficiency at 303K and 333K, respectively indicating excellent inhibition potential. Further increase in the concentration of ATA may afford higher inhibition efficiency, but this could be ascertained by further studies.

3.5 Adsorption kinetics

In order to describe the mode of adsorptive interaction between the ATA molecules and the steel surface, the degree of surface coverage was estimated from inhibition efficiency values and the obtained fractional surface coverage data were fitted into various adsorption isotherm models described in literature [32]. The Langmuir model afforded best fit with the highest adjusted and Pearson's R^2 values on linearization of the plots (Fig. 3a). This model maybe extrapolated to examine the dependence of concentration of ATA molecules (C) on its fractional coverage (θ) on the steel surface according to equation (16).

$$\frac{C}{\theta} = nC + \frac{n}{K_{ads}} \tag{16}$$

where n is the monolayer correction factor representing the number of ATA molecules adsorbed per active site of the steel surface and K_{ads} is the reciprocal of adsorption-desorption equilibrium constant. The values of ΔG_{ads} are related to the free energy of adsorption by equation (17).

$$\Delta G_{ads} = -RT\ln 55.5 K_{ads} \tag{17}$$

where R is the universal gas constant and T is the absolute temperature.

Results obtained from analyses of data reveal that n values were between 1.02 and 1.12. This indicated that approximately one molecule of ATA occupied a given adsorption site, hence monolayer adsorption or

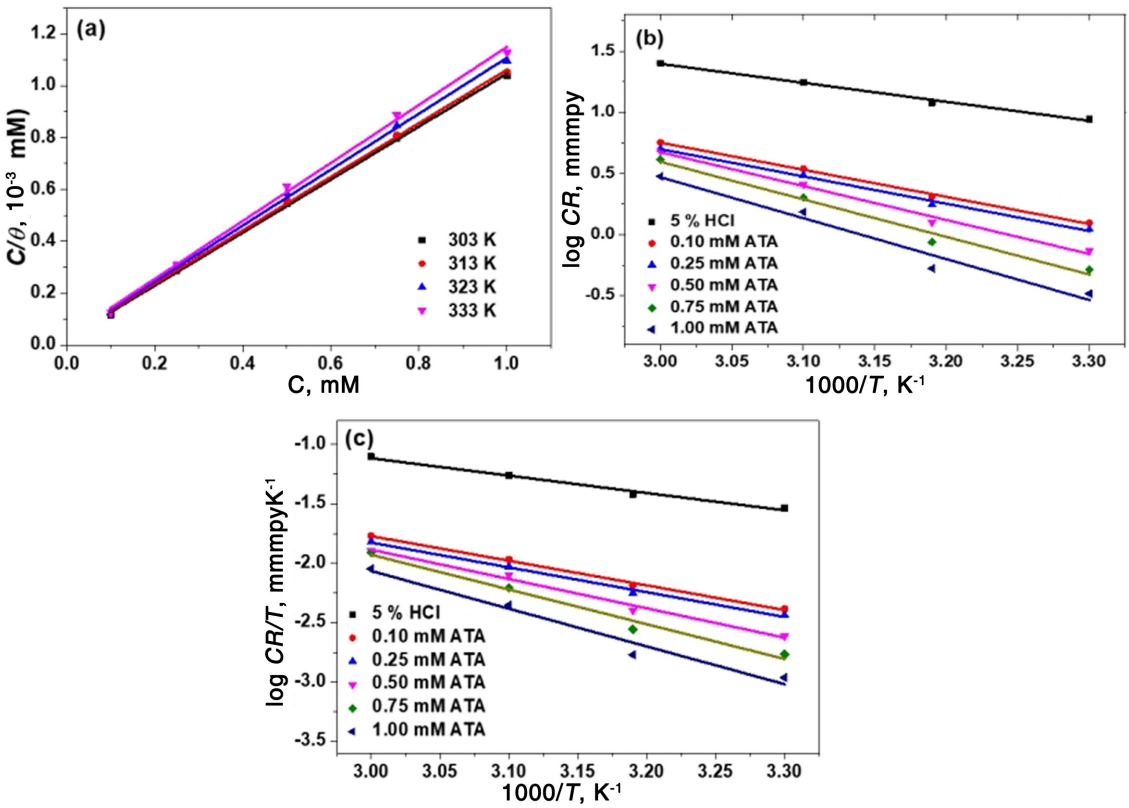

Fig. 3. (a) Langmuir adsorption isotherm (b) Arrhenius plots and (c)Transition state plots for the corrosion of X80 steel surface in 5% HCl without and with different concentration of ATA at different temperatures

Table 4. Some adsorption-related parameters calculated from Langmuir isotherm

T (K)	Slope	R^2	K_{ads} (10^4 mM^{-1})	ΔG_{ads} (kJ/mol)
303	1.02±0.015	0.9997	3.85	-36.71
313	1.03±0.017	0.9996	3.33	-36.35
323	1.07±0.020	0.9995	3.23	-36.27
333	1.12±0.018	0.9991	3.12	-36.19

chemisorption mechanism. The predicted chemical adsorption mode was further supported by the obtained values of ΔG_{ads} (Table 4) which were more negative than -20 kJ/mol. Thus, the adsorbed ATA molecules may have formed actual coordinate covalent bonds by back-donation of its electrons to the empty *d*-orbitals of Fe on the steel surface. More insights into this mode of adsorption was further investigated by computational studies. The values of K_{ads} obtained decreased slightly when the temperature increased, indicating a possibility of desorption of some ATA molecules at higher temperatures, hence slight reduction in magnitude of inhibition efficiency.

3.6 Thermodynamic studies

Thermodynamic studies was employed to predict the effect of temperature on the collision of molecules on the steel surface, corrosion rate and activation energy. Arrhenius equation (18) and Transition state equation (19), which relate the corrosion rate as a function of temperature to the thermodynamic parameters of interest, were deployed.

$$\log CR = \log Z - \frac{E_a}{2.303RT} \tag{18}$$

$$\log\left(\frac{CR}{T}\right) = \left[\left(\log\left(\frac{R}{Nh}\right)\right) + \left(\frac{\Delta S^*}{2.303R}\right) - \left(\frac{\Delta H^*}{2.303RT}\right)\right] \tag{19}$$

where corrosion rate is denoted by *CR*, Z denotes Arrhenius frequency constant of pre-exponential, *h* is Planck's constant, *N* is Avogadro's constant, *T* is the absolute temperature, ΔS^* and ΔH^* are the entropy and enthalpy of activation, respectively.

The plots obtained from fitting experimental data into these models are shown in Fig. 3b and 3c respectively whereas the activation parameters deduced from analyses of the plots are displayed in Table 5. Fundamentally, the acid molecules initially drift from the bulk solution towards the steel surface where they collide and cause corrosive attack thereof. In the same way, ATA molecules also drift towards and condense on the surface for adsorption to occur. The minimum barrier of energy that the acid molecules must overcome to attack the steel surface and corrode it is a measure of the activation energy. The E_a determined without the inhibitor was 0.297 kJ/mol but this energy barrier increased to 0.423 kJ/mol and 0.640 kJ/mol in the solutions containing 0.10 mm ATA and 1.00 mm ATA, respectively. Thus, adsorption of the inhibitor increases the activation energy, which in turn reduces the corrosion rate. The values of ΔS^* obtained were all negative indicating that there was a decrease in molecular random motion caused by adsorptive association between ATA molecules and steel surface. In the same way, the values of ΔH^* were all negative indicating that ATA adsorption was exothermic, similar to other adsorption processes [32]. Thermodynamically, negative large ΔH^* values and negative (small) ΔS^* values are consistent with negative ΔG^* values indicating spontaneous adsorption of ATA on steel surface at all temperatures.

3.7 Surface morphological analyses

For comparison, the SEM images of the steel surface retrieved from the 5% HCl without ATA (a) was placed side by side with the steel surface retrieved from the solution containing 1.00 mM ATA (b) as shown in Fig. 4.

The surface (Fig. 4a) is characterized with high degree of roughness due to uncontrolled corrosive attack by the acid solution. Although the surface (Fig. 4b) has some degree of roughness, it is smoother compared to (Fig 4a) due to protective effect of adsorbed ATA molecules. EDAX result (Table 6) revealed that adsorption of ATA on the surface resulted in increase in the amounts of C, N and O atoms on the steel surface compared to the free acid solution. These atoms are distributed at various locations on the surface as depicted in the EDAX map of the surfaces (Figs. 4c and 4d). The presence of these atoms on the surface could only have been facilitated

Table 5. Some kinetic and thermodynamic parameters calculated from Arrhenius and transition state plots

Test solution	E_a (kJ/mol)	$-\Delta H_{ads}$ (kJ/mol)	$-\Delta S_{ads}$ (kJ/mol)
5 % HCl	0.297	27.656	0.133
0.10 mM ATA	0.423	39.290	0.112
0.25 mM ATA	0.428	39.479	0.111
0.50 mM ATA	0.530	46.706	0.092
0.75 mM ATA	0.587	55.370	0.066
1.00 mM ATA	0.640	60.118	0.054

Table 6. Elemental composition on the surface of retrieved steel coupons determined by EDAX

Element	Surface retrieved from uninhibited 5% HCl solution		Surface retrieved from inhibited 5% HCl solution of 1.0 mM ATA	
	Atom (%)	Weight (%)	Atom (%)	Weight (%)
Fe	72.18	54.36	61.40	46.92
C	21.63	31.07	26.08	32.16
N	-	-	2.42	5.09
O	4.84	11.82	9.82	14.28
Cl	1.36	2.75	0.28	1.55

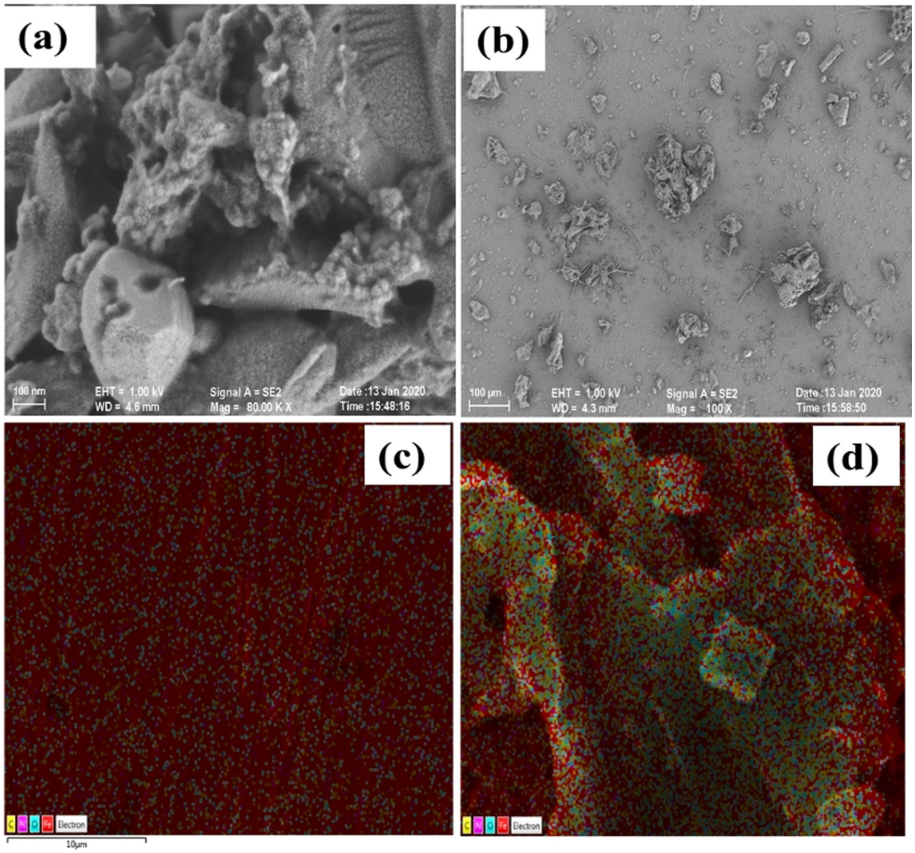

Fig. 4. SEM images of X80 steel surface immersed in (a) 5% HCl and (b) 5 % HCl containing 1.0 mM ATA and EDAX maps showing distribution of atoms on the surface of steel retrieved from (c) 5% HCl and (d) 5 % HCl containing 1.0 mM ATA

by surface adsorbed ATA molecules. Perhaps, on adsorption, the molecules of ATA displaced Cl^- ions on the surface resulting in lower amounts of Cl compared to the surface in the uninhibited HCl solution.

3.8 Computational studies

The optimized structure of ATA using DFT/6-311G(d,p) is displayed in Fig. 1b. This structure depicts the one with minimum energy and was used throughout for all computations.

3.8.1 Quantum chemical properties of ATA and the effects of solvation

Quantum chemical parameters can offer useful insights into the molecular properties and energetic stability or reactivity of inhibitors. These parameters were computed and used to assess and describe the robustness of ATA inhibitor and the results are displayed in Table 7.

Most corrosion processes occur in an aqueous medium, impacting the inhibitor's ability to form a protective layer on the steel surface. Understanding the effect of solvation is crucial in assessing key performance indices of the inhibitor. In Table 7, solvation demonstrates a significant impact on the quantum chemical properties of ATA, particularly on E_{gap}, which is a key determinant of the reactivity index of the inhibitor.

The E_{gap} slightly increases from 0.179 eV to 0.181 eV when transitioning from the gaseous phase to the aqueous phase. Despite the modest change, this elevation plays a crucial role in augmenting the reactivity of ATA in the solution. A lower E_{gap} in the aqueous phase would imply greater stabilization of the inhibitor in the medium, potentially adversely affecting its adsorption potential on the metal surface. It is noteworthy that the aqueous phase primarily acts as a dispersive medium; any stabilization within it would influence the adsorption characteristics, impacting the efficiency of the inhibitor in forming a stable and protective film on the metal. Our

Table 7. Quantum chemical parameters for ATA in gaseous and aqueous phases

ATA	E_{HOMO} (eV)	E_{LUMO} (eV)	E_{gap} (eV)	IE (eV)	EA (eV)	χ (eV)	η (eV)	σ (eV^{-1})	ΔN
With solvent	-0.260	-0.079	0.181	0.260	0.079	0.170	0.091	10.989	25.549
Without solvent	-0.256	-0.077	0.179	0.256	0.077	0.166	0.090	11.111	25.856

result reveals otherwise, and the solvation-induced increase in E_{gap} proves satisfactory in enhancing the interaction between the inhibitor and the metal surface.

Another key parameter is electronegativity which is a vital quantum chemical parameter that influences corrosion inhibition. It measures an atom's tendency to attract a bonding pair of electrons, significantly impacting adsorption. Molecules with higher electronegativity tend to form robust bonds with metal surfaces, facilitated by available electron density for interaction. In the case of ATA, solvation enhances electronegativity from 0.166 eV to 0.170 eV. This observed increase signifies that a solvated ATA molecule will exhibit stronger adsorption on the steel surface.

The highest occupied molecular orbital (HOMO) and lowest unoccupied molecular orbital (LUMO) energies play a crucial role in molecular interactions with metal surfaces. The HOMO, representing the highest energy level occupied by electrons in a molecule, determines the inhibitor's tendency to donate electrons to the metal surface. A higher-lying HOMO indicates a greater electron-donating propensity. However, in the case of ATA, solvation diminishes this tendency. On the other hand, the LUMO, the lowest unoccupied orbital, is involved in accepting electrons from the metal surface. Solvation enhances this tendency favourably, as evidenced by a lower value in the aqueous phase compared to the gaseous phase.

Global softness and global hardness play pivotal roles in understanding the reactivity and stability of molecules, especially concerning corrosion inhibition. Global hardness represents a molecule's resistance to changes in electronic density, indicating stability. On the other hand, global softness, which measures polarizability, reflects a molecule's reactivity. These quantum chemical parameters offer valuable insights in that, molecules with higher global hardness tend to be more stable and less reactive, making them potential candidates for corrosion inhibitors. Conversely, molecules with higher global softness are less stable and more reactive, which may impact their effectiveness in inhibiting corrosion processes.

In the aqueous phase, ATA exhibits higher global hardness, indicating its hardness in this medium. The lower reactivity of ATA in the aqueous phase is advantageous since the aqueous medium is required for dispersion purposes, thus facilitating better adsorption behaviour on the Fe(110) surface. These characteristics ensure that ATA interacts maximally with the metal surface rather than the aqueous medium. The elevated global hardness of ATA in the aqueous phase favours its interaction with the Fe(110) surface, contributing to its corrosion inhibition effectiveness

3.8.2 Frontier molecular orbitals

Frontier molecular orbitals of inhibitor provide a clear picture about the centres, regions, bonds and atoms involved in adsorption/inhibition process. It also indicates the spread of these centres within the inhibitor molecule. The HOMO and LUMO orbitals of ATA are shown in Fig. 5a and 5b, respectively. The HOMO represents the electron donating character of the inhibitor and these are primarily the electron rich aromatic rings as depicted by the lobes. The steel surface receives electron donation through the HOMO centres or regions. The LUMO represents the electron accepting ability, usually receiving feedback donation from the metal surface to the inhibitor.

The HOMO and LUMO visualization plots can provide valuable insights into regions of the inhibitor involved in interaction with a metal surface. Potential interaction sites are regions where the HOMO and LUMO have significant overlap. As shown in Fig. 5, the HOMO and LUMO are well spread across the entire ATA molecule except O16 and O20. Such distribution of HOMO and LUMO centres is consistent with strong

adsorption of ATA on the steel surface. It is noteworthy that the oxygen atoms of the carboxylic acid group neither contribute to the LUMO nor HOMO centres. It can be inferred therefore that the carboxylic acid group has no contribution to the inhibition properties of ATA. It is simply isolated from the inhibition process. Any atom that does not show either HOMO or LUMO centre can be considered non-participatory in the adsorption of any inhibitor on a metal surface leading to corrosion mitigation. Significant contributions to HOMO and LUMO are highlighted by large orbital lobes and an overlay of HOMO and LUMO plots reveal overlapping of HOMO and LUMO regions marking potential interaction sites with the metal surface.

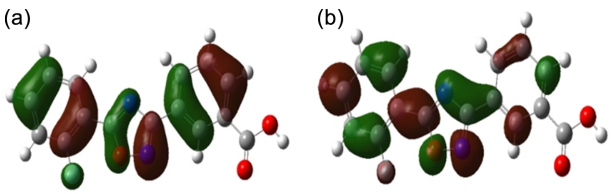

Fig. 5. Visual representation of molecular orbitals of ATA (a): HOMO; and (b): LUMO

3.8.3 Solvation effect on ATA's charge distribution and reactivity sites

The inclusion of solvent effects in Density Functional Theory (DFT) calculations is crucial due to the significant impact of the solvent medium on various properties. This encompasses heats of formation, heats of reaction, dipole moments, and other electronic properties. In the study of the corrosion inhibition of ATA, the solvent effect on the distribution of Fukui indices and Mulliken charge

Table 8. Fukui Indices and Mulliken charge distribution of ATA

Atom	Nucleophilic (gaseous) $f_k^{(+)}$	Nuclephilic (aqueous) $f_k^{(+)}$	Electrophilic (gaseous) $f_k^{(-)}$	Electrophilic (aqueous) $f_k^{(-)}$	Mulliken charges (gaseous)	Mulliken charges (aqueous)
C1	0.070	0.080	0.038	0.055	-0.056	-0.063
C2	0.010	0.017	0.013	0.025	-0.038	-0.047
C3	0.032	0.048	0.020	0.043	0.066	0.063
C4	0.026	0.031	0.035	0.058	0.080	0.078
C5	0.034	0.050	0.010	0.022	-0.066	-0.074
C6	0.012	0.021	0.031	0.059	-0.065	-0.074
C7	0.078	0.108	0.025	0.030	0.432	0.447
O8	0.043	0.054	0.030	0.031	-0.383	-0.397
N9	**0.095**	**0.111**	**0.105**	**0.102**	-0.059	-0.105
C10	0.039	0.054	0.035	0.036	0.230	0.244
N11	0.053	0.057	0.042	0.041	-0.347	-0.360
C12	-0.005	0.004	0.015	0.022	0.097	0.092
C13	0.020	0.032	0.022	0.026	-0.092	-0.097
C14	0.008	0.004	0.010	0.008	0.015	0.008
C15	0.023	0.022	0.037	0.036	-0.101	-0.100
C16	0.013	0.015	0.016	0.019	-0.062	-0.072
C17	-0.000	0.009	0.011	0.016	-0.096	-0.098
C18	0.010	0.007	0.012	0.008	**0.563**	**0.576**
O19	0.019	0.008	0.024	0.009	-0.439	-0.508
O20	0.018	0.005	0.021	0.006	**-0.459**	**-0.483**
Cl21	0.088	0.064	**0.124**	**0.136**	-0.159	-0.184

Parameters for H atoms are excluded as none was indicated with highest value of the calculated functions

distribution was probed by recording values in both gaseous and aqueous phase and detailed result of this investigation is documented in Table 8.

Fukui indices, encompassing Fukui electrophilic $f_k^{(-)}$ and Fukui nucleophilic $f_k^{(+)}$, serve as predictive tools for identifying reactive sites of inhibitors during metal surface adsorption. These indices evaluate nucleophilic and electrophilic characteristics at various atomic positions, assigning elevated values to predisposed sites. In the case of ATA, the Fukui nucleophilic index designates N9, highlighting its proclivity to donate electrons for favourable interactions with positively charged species on the metal surface. Conversely, the Fukui electrophilic index peaks at Cl21, indicating a pronounced tendency to accept electrons during interactions with negatively charged species. Notably, solvation has minimal impact on the highly reactive sites identified by Fukui indices. The consistent high reactivity of the same atom in both gaseous and aqueous phases underscores stability despite solvent presence.

Mulliken atomic charges provide insights into the distribution of charge on atoms individually within a molecule. As observed, atom C18 exhibits the highest positive Mulliken charge within the molecule, while atom O20 exhibits the highest negative Mulliken charge. A noteworthy trend is observed in the distribution of charges as the system transitions from the gaseous to the aqueous phase. There is a discernible increase in charge from the gaseous phase to the aqueous phase. This observed trend indicates an augmented interaction strength between ATA and the steel surface in the aqueous environment. The variations in Mulliken charges indicate changes in the electronic structure, emphasizing the significance of solvent effects on the molecule's reactivity and its potential impact on corrosion inhibition.

3.9 Molecular dynamics simulation

Molecular dynamics approach was used to simulate and study the electronic structure and energetics of the adsorption of ATA on steel surface. At the atomic and molecular level, it provides insights into the nature of interaction and configuration of the inhibitor on the metal surface. The result of the configuration of ATA on Fe(110) surface is shown in Fig. 6.

The Connolly surface, illustrated in Fig. 6a, delineates the spatial domain occupied by the Fe atoms, accessible to the inhibitor solution. The entirety of the inhibitor solution components is presumed to be encapsulated within the Connolly surface. This design guarantees the continuous submersion of the Fe surface in the inhibitor solution throughout molecular dynamics studies. Notably, ATA demonstrates a planar configuration on the Fe surface, a critical factor for optimizing the alignment of HOMO and LUMO centres, thereby facilitating robust adsorption. The persistence of this configuration across all investigated temperatures indicates the consistent binding mode of ATA.

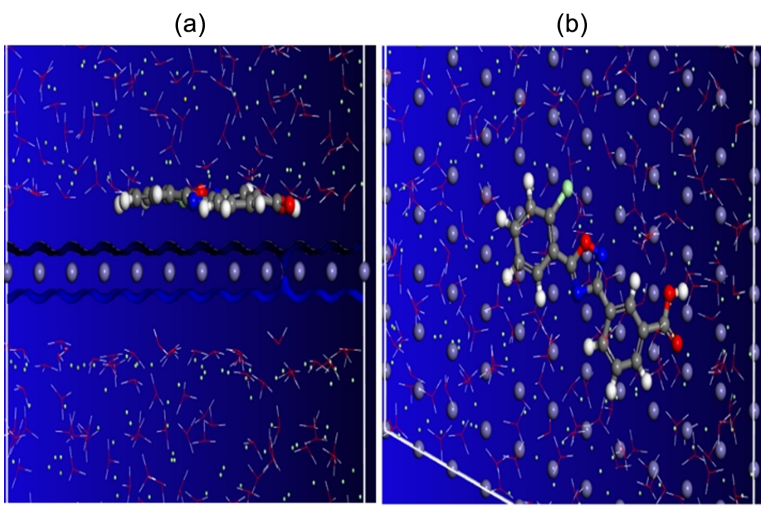

Fig. 6. Configuration of ATA on (Fe(110) surface, (a): Side view; (b): Top view. [O: red; N: blue; C: grey; H: white; Cl: light green]

3.9.1 Interaction energy of ATA on Fe(110) surface

Interaction energy is a crucial parameter that quantifies the strength of interaction between an inhibitor and a metal surface. The magnitude and sign of this interaction energy play a pivotal role in predicting the adsorption behaviour and the mechanism of adsorption. In the context of ATA (an inhibitor) on a steel surface, specifically represented by the Fe(110) surface, a comprehensive study was conducted at various temperatures within the range of 303 - 333 K. The results of this investigation presented in Table 9, provide valuable insights into how the strength of interaction between ATA and the steel surface varies under different temperature conditions.

The results obtained reveal a notable increase in interaction energy, upon the introduction of ATA into the solution. Specifically, at 30 ºC, the interaction energy in the acid solution alone is considerably low at -471.39 kcal/mol. However, with the addition of ATA, the energy increases to -114.30 kcal/mol. Elevated interaction energies are indicative of stronger adsorption, a critical factor for enhancing the corrosion efficiency of inhibitors relying on adsorption mechanisms, particularly in protecting metal surfaces. The negative sign of the interaction energy signifies an exothermic process, and supports experimental results.

Investigating the impact of temperature on interaction energy and inhibition efficiency provides crucial insights into the underlying corrosion inhibition mechanism. Interaction energy between ATA and the Fe(110) surface initially rises from 303 ºC reaching its peak at 313 ºC. Subsequently, further increase in temperature causes a decline in interaction energy. Inhibition efficiency of ATA mirrors a similar pattern, escalating from 75.8% to 76.1% within the temperature range of 303 - 313 ºC. However, it experiences a decline to 74.6% as the temperature drops to 333 K. The optimal temperature for ATA's inhibition efficiency is identified as 313 K, aligning with the highest interaction energy. The initial rise in inhibition efficiency from 303 - 313 K signifies a chemisorption-dominated process, while the decline from 313-333 K indicates a shift towards physisorption. This behaviour which can be characterized as a mixed-type behaviour, is typical of most organic inhibitors [14,33] and is consistent with experimental inference from electrochemical studies. Overall, the observed inhibition efficiency of 74.6-76.1% at different temperatures establishes ATA as an effective corrosion inhibitor for steel in 5% HCl solution.

3.9.2 Distribution of binding energies

Binding energy is a measure of the energy or strength of interaction between any two or more components that are bound together. The distribution of binding energy can provide valuable information on adsorption sites associated with the adsorptive binding of ATA to Fe (110) surface. Higher binding energy at specific sites is indication of energetically favourable interaction. The distribution of the binding energy of ATA on Fe(110) surface is shown in Fig. 7. This was recorded using Blend Module of Materials Studio with a sampling energy of 1.0×10^6 and energy band width of 0.2 kcal/mol. The screen role was assigned to ATA while the base role was assigned to Fe(110) surface.

The energy distribution reveals two prominent active sites characterized by higher binding energy. Enhanced reactivity on these sites is implied, considering that adsorption typically occurs at active sites with elevated binding energy. Upon examining the structure of ATA, it becomes apparent that it contains two types of heteroatoms: nitrogen and oxygen. Previous studies [34] have highlighted heteroatoms as potential adsorption points for organic inhibitors. Consequently, it is evident

Table 9. Interaction energy and inhibition efficiency of ATA on Fe(110) surface at different temperatures

Temp (K)	Interaction energy without inhibitor E_o (kcal/mol)	Interaction energy with inhibitor E_{int} (kcal/mol)	Inhibition efficiency (E_{inh}%)
303	-471.387	-114.305	75.8
313	-471.799	-112.721	76.1
323	-457.844	-113.928	75.1
333	-446.699	-113.529	74.6

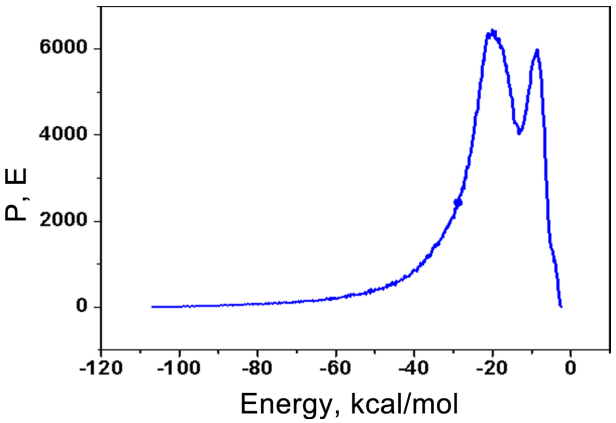

Fig. 7. Binding energy distribution of ATA on Fe(110) surface

that the major active sites of ATA are the nitrogen and oxygen atoms within the oxadiazole ring, since the oxygen atoms in the carboxylic acid group play no participatory roles.

4. Conclusion

This study explores the potential of ATA as a novel corrosion inhibitor for X80 steel in a simulated acid wash solution. Results reveal that ATA efficiently inhibited X80 steel corrosion especially at 303 K and 313 K. The efficiency of inhibition was dependent on temperature and ATA concentration – increasing with increase concentration but decreasing with increase in temperature. Addition of ATA to the 5% HCl resulted in increase in charge transfer resistance indicating the adsorption and formation of a protective ATA film on the steel surface. Adsorption and simulation studies reveal that the adsorption of ATA molecules on X80 steel surface occurred via a combination of chemical and physical adsorption mechanisms. The primary active adsorption sites on ATA are identified as the nitrogen and oxygen atoms in the oxadiazole ring. However, at high temperatures above 60 ºC studied, the efficiency of ATA may decline overtly and would therefore require to be optimized by blending with some synergistic additives to obtain a corrosion inhibitor for oilfield acid wash operations.

Acknowledgements

The experimental section of this research work was supported by the National Natural Science Foundation of China (No. 52074232) and Sichuan Science and Technology Program (No. 2022NSFSC0028). The computational section was supported by the TETFund Center of Excellence in Computational Intelligence, University of Uyo, Nigeria. The authors appreciate and acknowledge all the support.

References

1. M. Finšgar and J. Jackson, Application of corrosion inhibitors for steels in acidic media for the oil and gas industry: A review, *Corrosion Science,* **86**, 17 (2014). Doi: https://doi.org/10.1016/j.corsci.2014.04.044
2. Johannes Fink, Petroleum engineer's guide to oil field chemicals and fluids, 2nd ed., Gulf Professional Publishing, ISBN: 978-0-323-85438-2 (2021).
3. H. W. Muslim, A. M. Mustafa and F. F. Sayyid, Corrosion protection effectiveness and adsorption performance of whey inhibitor with cocoa for mild steel in hydrochloric acid environment, *Corrosion Science and Technology,* **23**, 343-351 (2024). Doi: https://doi.org/10.14773/cst.2024.23.5.343
4. M. Askari, M. Aliofkhazraei, R. Jafari, P. Hamghalam and A. Hajizadeh, Downhole corrosion inhibitors for oil and gas production–a review, *Applied Surface Science Advances,* **6**, 100128 (2021). Doi: https://doi.org/10.1016/j.apsadv.2021.100128
5. A. A. Olajire, Corrosion inhibition of offshore oil and gas production facilities using organic compound inhibitors-A review, *Journal of Molecular Liquids,* **248**, 775 (2017). Doi: https://doi.org/10.1016/j.molliq.2017.10.097
6. Z. Shang and J. Zhu, Overview on plant extracts as green corrosion inhibitors in the oil and gas fields, *Journal of Materials Research and Technology,* **15**, 5078 (2021). Doi: https://doi.org/10.1016/j.jmrt.2021.10.095
7. K. Tamalmani and H. Husin, Review on corrosion inhibitors for oil and gas corrosion issues, *Applied Sciences*, **10**, 3389 (2020). Doi: https://doi.org/10.3390/app10103389
8. E. Ituen, O. Akaranta and S. A. Umoren, N-acetyl cysteine based corrosion inhibitor formulations for steel protection in 15% HCl solution, *Journal of Molecular Liquids,* **246**, 112 (2017). Doi: https://doi.org/10.1016/j.molliq.2017.09.040
9. W. Zhao, F. Li, X. Lv, J. Chang, S. Shen, P. Dai, Y. Xia and Z. Cao. Research progress of organic corrosion inhibitors in metal corrosion protection, *Crystals*, **13**, 1329 (2023): Doi: https://doi.org/10.3390/cryst13091329

10. H. Parangusan, M. H. Sliem, A. M. Abdullah, M. Elhaddad, N. Al-Thani, and J. Bhadra, Plant Extract as Green Corrosion inhibitors for Carbon steel substrate in different environments: A systematic review, *International Journal of Electrochemical Science,* **20**, 100919 (2024). Doi: https://doi.org/10.1016/j.ijoes.2024.100919
11. E. Landfeldt, T. Sejersen and M. Tulinius, A mini-review and implementation model for using ataluren to treat nonsense mutation Duchenne muscular dystrophy, *Acta Paediatrica*, **108**, 224 (2019). Doi: https://doi.org/10.1111/apa.14568
12. S. W. Peltz, M. Morsy, E. M. Welch and A. Jacobson, Ataluren as an agent for therapeutic nonsense suppression, *Annual Review of Medicine,* **64**, 407 (2013). Doi: https://doi.org/10.1146/annurev-med-120611-144851
13. N. Wang, X. Liu and D. Jiang, Preparation of Isoetes sinensis extract as a green corrosion inhibitor for Q235 carbon steel in hydrochloric acid, *International Journal of Electrochemical Science,* **17**, 221266 (2022). Doi: https://doi.org/10.20964/2022.12.67
14. E. Ituen, V. Mkpenie and E. Ekemini, Corrosion inhibition of X80 steel in simulated acid wash solution using glutathione and its blends: Experimental and theoretical studies, *Colloids and Surfaces A: Physicochemical and Engineering Aspects,* **578**, 123597 (2019). Doi: https://doi.org/10.1016/j.colsurfa.2019.123597
15. ASTM G1-03 Standard Practice for Preparing, Cleaning, and Evaluating Corrosion Test Specimens, ASTM International (2017).
16. E. Ituen, J. Asuquo, L. Yuanhua and O. Akaranta, Adsorption of cowpea husk extract and corrosion inhibition at interface between X80 steel and acidic oilfield descaling fluid, *Letters in Applied NanoBioScience*, **12**, 122 (2022). Doi: https://doi.org/10.33263/LIANBS124.122
17. M. Mobin, I. Ahmad, M. Murmu, P. Banerjee and R. Aslam, Corrosion inhibiting properties of polysaccharide extracted from Lepidium meyenii root for mild steel in acidic medium: Experimental, density functional theory, and Monte Carlo simulation studies, *Journal of Physical Chemistry of Solids*, **179**, 111411 (2023). Doi: https://doi.org/10.1016/j.jpcs.2023.111411
18. Z. Ahmad, Principles of corrosion engineering and corrosion control, Elsevier, ISBN: 13-978-0-7506-5924-6 (2006).
19. E. Ituen, A. Singh, L. Yuanhua and O. Akaranta, Green synthesis and anticorrosion effect of Allium cepa peels extract-silver nanoparticles composite in simulated oilfield pickling solution, *SN Applied Sciences,* **3**, 679 (2021). Doi: https://doi.org/10.1007/s42452-021-04670-w
20. C. Lee, W. Yang and R. G. Parr, Development of the colle-salvetti correlation energy formula into a functional of the electron density, *Physical Review*, ***B*37**, 785 (1988). Doi: https://doi.org/10.1103/PhysRevB.37.785
21. M. J. Frisch, G. W. Trucks, H. B. Schlegel, G. E. Scuseria, M. A. Robb, J. R. Cheeseman, G. Scalmani, V. Barone, B. Mennucci, G. A. Petersson, Gaussian 09, Revision A.02, Gaussian Inc., Wallingford CT (2009).
22. E. Cances and B. Mennucci, New applications of integral equations methods for solvation continuum models: ionic solutions and liquid crystals, *Journal of Mathematical Chemistry*, **23**, 309 (1998). Doi: https://doi.org/10.1023/A:1019133611148
23. Z. Cao, Y. Tang, H. Cang, J. Xu, G. Lu and W. Jing, Novel benzimidazole derivatives as corrosion inhibitors of mild steel in the acidic media. Part II: theoretical studies, *Corrosion Science,* 83, 292-298 (2014). Doi: https://doi.org/10.1016/j.corsci.2014.02.025
24. N. B. Iroha, V. C. Anadebe, N. J. Maduelosi, L. A. Nnanna, L. C. Isaiah, O. Dagdag, A. Berisha and E. E. Ebenso, Linagliptin drug molecule as corrosion inhibitor for mild steel in 1 M HCl solution: Electrochemical, SEM/XPS, DFT and MC/MD simulation approach, *Colloids and Surfaces A: Physicochemical and Engineering Aspects*, **660**, 130885 (2023). Doi: https://doi.org/10.1016/j.colsurfa.2022.130885
25. N. D. Nam, H. P. Van, N. T. Hoai and V. T. H. Thu, A study on the mixed corrosion inhibitor with a dominant cathodic inhibitor for mild steel in aqueous chloride solution, *Journal of Taiwan Institute of Chemical Engineers*, **91**, 556 (2018). Doi https://doi.org/10.1016/j.jtice.2018.06.007
26. A. A. El-Feki and G. W. Walter, Corrosion rate measurements under conditions of mixed charge transfer plus diffusion control including the cathodic metal ion deposition partial reaction, *Corrosion Science*, **42**, 1055 (2000). Doi: https://doi.org/10.1016/S0010-938X(99)00120-1
27. K. H. Rashid, A. A. Khadom, H. B. Mahood and A. N. Campbell, The effect of mass transfer on corrosion in oilfield production processes by wastewater enriched with CO_2: Computer-aided modeling and experimental verification, *Case Studies in Chemical and Environmental Engineering*, **2**, 100030 (2020). Doi: https://doi.org/10.1016/j.cscee.2020.100030
28. E. Ituen, L. Yuanhua, C. Verma, A. Alfantazi, O. Akaranta and E. E. Ebenso, Synthesis and characterization of walnut husk extract-silver nanocomposites for

removal of heavy metals from petroleum wastewater and its consequences on pipework steel corrosion, *Journal of Molecular Liquids*, **335**, 116132 (2021). Doi: https://doi.org/10.1016/j.molliq.2021.116132

29. R.T. Loto, Evaluation of the corrosion inhibition effect of the combined admixture of rosemary and cinnamon cassia oil on mild steel in weak acid electrolyte, *Sustainable Chemistry and Pharmacy,* **17**, 100298 (2020). Doi: https://doi.org/10.1016/j.scp.2020.100298
30. N. D. Nam, P. Van Hien, N. T. Hoai and V. T. H. Thu, A study on the mixed corrosion inhibitor with a dominant cathodic inhibitor for mild steel in aqueous chloride solution, *Journal of Taiwan Institute of Chemical Engineers*, **91**, 556 (2018). Doi: https://doi.org/10.1016/j.jtice.2018.06.007
31. S. Mo, I. J. Li, H.Q. Luo and N. B. Li, An example of green copper corrosion inhibitors derived from flavor and medicine: Vanillin and isoniazid, *Journal of Molecular Liquids,* **242**, 822 (2017). Doi: https://doi.org/10.1016/j.molliq.2017.07.081
32. E. Ituen, O. Akaranta and A. James, Evaluation of performance of corrosion inhibitors using adsorption isotherm models: an overview, *Chemical Science International Journal*, **18**, 1 (2017). Doi: https://doi.org/10.9734/CSJI/2017/28976
33. N. O. Eddy, P. O. Ameh and N. B. Essien, Experimental and computational chemistry studies on the inhibition of aluminium and mild steel in 0.1M HCl by 3-nitrobenzoic acid, *Journal of Taibah University of Sciences*, **12**, 545 (2018). Doi: https://doi.org/10.1080/16583655.2018.1500514
34. D. Q. Huong, T. Duong and P. C. Nam, Experimental and theoretical study of corrosion inhibition performance of N-phenylthiourea for mild steel in hydrochloric acid and sodium chloride solution, *Journal of Molecular Modelling,* **25**, 204 (2019). Doi: https://doi.org/10.1007/s00894-019-4084-6